Editors' Suggestion

Giant Thermoelectric Response of Nanofluidic Systems Driven by Water Excess Enthalpy

Li Fu, Laurent Joly,* and Samy Merabia†
Univ Lyon, Univ Claude Bernard Lyon 1, CNRS, Institut Lumière Matière, F-69622 Villeurbanne, France

(Received 21 April 2019; revised manuscript received 11 July 2019; published 24 September 2019)

Nanofluidic systems could in principle be used to produce electricity from waste heat, but current theoretical descriptions predict a rather poor performance as compared to thermoelectric solid materials. Here we investigate the thermoelectric response of NaCl and NaI solutions confined between charged walls, using molecular dynamics simulations. We compute a giant thermoelectric response, 2 orders of magnitude larger than the predictions of standard models. We show that water excess enthalpy—neglected in the standard picture—plays a dominant role in combination with the electro-osmotic mobility of the liquid-solid interface. Accordingly, the thermoelectric response can be boosted using surfaces with large hydrodynamic slip. Overall, the heat harvesting performance of the model systems considered here is comparable to that of the best thermoelectric materials, and the fundamental insight provided by molecular dynamics suggests guidelines to further optimize the performance, opening the way to recycle waste heat using nanofluidic devices.

DOI: 10.1103/PhysRevLett.123.138001

Introduction.—With a fast-growing energy consumption, and energy production based mostly on fossil fuels, our society is in crucial need of new, sustainable energies. Nanofluidic systems could play a key role in the development of such new energies [1,2]. For instance, blue energy systems based on membranes with nanoscale porosity can produce electricity from salinity difference with very good efficiency, opening the way to large-scale harvesting of the osmotic energy of sea water [3–5]. At the core of nanofluidic energy conversion systems lies the so-called electrokinetic (EK) effects, coupling different types of transport in nanochannels [6,7]. In aqueous electrolytes, EK effects arise from the dynamics of the electrical double layer (EDL), a diffuse layer of non-neutral liquid in the vicinity of charged surfaces, whose thickness—the Debye length λ_D—is typically nanometric in aqueous electrolytes [8–10].

EK energy conversion has been studied since the early 1960s, but it has found a renewed interest with the advent of nanofluidic systems, offering significant efficiency improvements [11,12], as predicted theoretically [13,14] and measured experimentally [15]. Hydroelectric energy conversion has been studied extensively in the past 15 years [5,16–19]. The increased performance arises from several mechanisms specific to the nanoscale [20], e.g., liquid-solid slip [1,21–23]. However, the possibility to use nanofluidic systems as thermoelectric converters has only been discussed very recently [24–29]. Traditional thermoelectric semiconductors offer high thermoelectric performance at room temperature, but their use is limited owing to their toxicity and rarity [26]. In that regard, EK effects have been studied and some analytical models have been suggested [26,30–36]. In particular, a recent theoretical study reported enhanced Seebeck coefficient in confined electrolyte solutions [30,31], an effect explained by the electrostatics of the EDL, in the spirit of a standard picture developed by Derjaguin and co-workers [37,38].

Here, we perform molecular dynamics (MD) simulations to explore the physical mechanisms at play in the thermoelectricity of nanofluidic channels, and we show that the thermoelectric response of confined electrolytes can be orders of magnitude higher than what is predicted by standard models.

Methods.—Under external gradients of electric potential $-\nabla U$ and of temperature $-\nabla T$, the thermoelectric response of a fluidic system can be described by the nondiagonal terms of the response matrix [39]:

$$\begin{bmatrix} j_e \\ j_h \end{bmatrix} = \begin{bmatrix} \sigma & M_{12} \\ M_{21} & \kappa T \end{bmatrix} \times \begin{bmatrix} -\nabla U \\ -\nabla T/T \end{bmatrix}, \tag{1}$$

where j_e is the electric current density, j_h is the heat flux density, σ and κ are the electrical and thermal conductivities of the system, and M_{ij} are phenomenological coefficients. M_{12} characterizes the so-called Seebeck effect—the conversion of heat into electricity, and M_{21} describes the Peltier effect—generation of an excess heat flux in an electric field. According to Onsager reciprocal relations, $M_{12} = M_{21} = M_{\mathrm{TE}}$ [39,40]. In the following, we will refer to M_{TE} as the thermoelectric coefficient.

We conducted MD simulations with LAMMPS [41] to compute the thermoelectric response of aqueous electrolyte solutions confined between two parallel Einstein solid walls (Fig. 1) and explored, in particular, the effect of surface charge. We considered two electrolytes, NaCl and NaI, which were shown to display different electro-osmotic

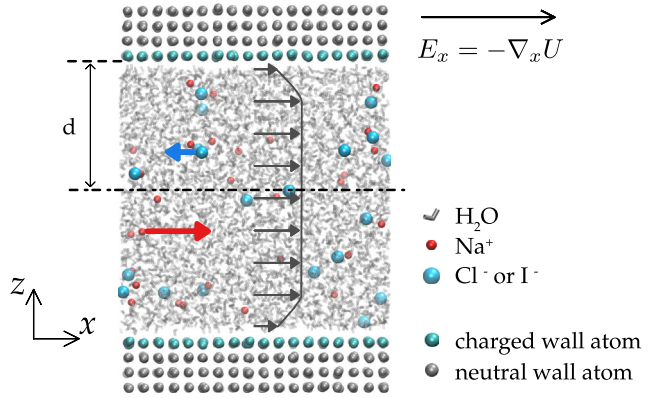

FIG. 1. Illustration of the simulation system. An aqueous electrolyte solution is confined in a slit nanochannel with charged inner surfaces. An external electric field is applied and the heat flux is computed. The arrows indicate the directions of ion motion.

(EO) responses due to ionic specificity [42,43]. We present here the main features of the simulations, and we report details in the Supplemental Material [44].

We used the TIP4P/2005 model [64] for water, and the scaled-ionic-charge model by Kann and Skinner [65] for ions. Liquid-solid interactions were taken from a previous MD study [42,43] of EO on a generic hydrophobic surface (contact angle ~140°), unless specified. We will come back to the large value of the contact angle in the following. Beyond the value of the surface charge, we explored the role of charge distribution by considering homogeneously or heterogeneously charged walls [44]. Counterions were added in the liquid to ensure electroneutrality.

The bulk electrolyte concentration ρ_b was set to ca. $0.35M$ unless specified (we will also present simulations without salt). This large salt concentration ensures that the Debye length, $\lambda_D \approx 5$ Å, is ~10 times smaller than the system height, so that the EDLs do not overlap.

To obtain the thermoelectric coefficient, we maintained the system at $T = 298$ K (applying a Nosé-Hoover thermostat to the liquid, only on the degrees of freedom perpendicular to the flow) and $p = 1$ atm [44], we applied different external electric fields $E_x = -\nabla_x U$ between 0.05 and 0.2 V/nm in independent simulations, and we computed the excess heat flux density j_h as detailed in previous work [66,67] and in Ref. [44]:

$$j_h = \frac{1}{2d}\int_{-d}^{d} \delta h(z) v(z) \mathrm{d}z, \tag{2}$$

where d is the half height of the channel, δh is the excess enthalpy density, and v is the velocity. The linearity of the response to the electric fields was checked and the linear regression of j_h against E_x gave the thermoelectric coefficient $M_{\mathrm{TE}} = M_{21} = j_h/E_x$. Note that the large electric fields considered here are commonly used in MD studies to extract the induced fluxes from thermal noise [42,43,68–72]; indeed, it has been shown that EK response coefficients obtained with such electric fields were consistent with equilibrium results obtained through the linear response theory, i.e., in the limit of vanishing forcing [69,73,74].

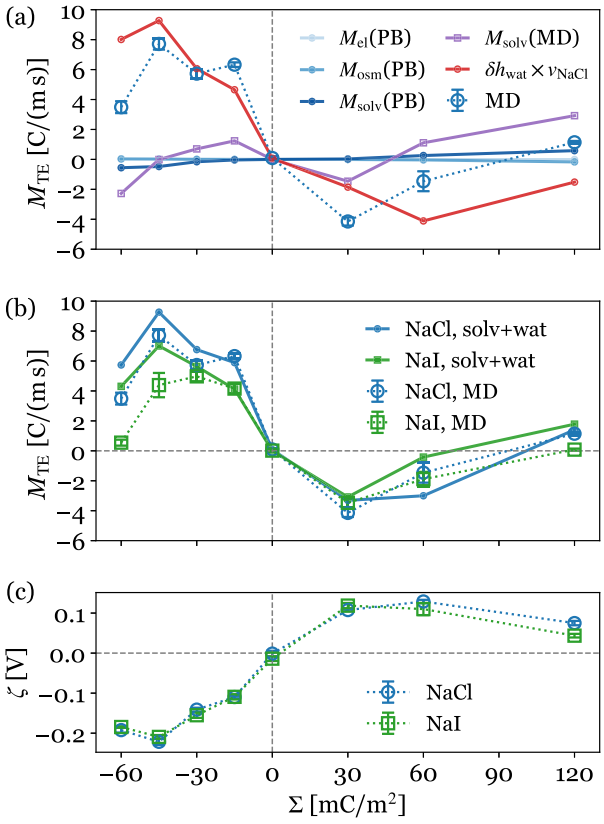

FIG. 2. (a) Thermoelectric coefficient M_{TE} as a function of the surface charge Σ, for NaCl solutions with homogeneously charged hydrophobic surfaces. Open symbols, MD results; solid lines, theoretical estimates of different contributions (see text for details). (b) M_{TE} vs Σ, comparison between NaCl and NaI. Open symbols, MD results; solid lines, model taking into account the water and solvation contributions (see text for details). (c) Computed ζ potential as a function of Σ for NaCl and NaI solutions.

Results and discussion.—Figures 2(a) and 2(b) display the evolution of the thermoelectric coefficient M_{TE} on a homogeneously charged hydrophobic surface as a function of the surface charge. For the two salts, $|M_{\mathrm{TE}}|$ goes through a maximum on both positively and negatively charged surfaces, and the dependency of M_{TE} against Σ is highly asymmetrical. Also, the response can be quite different for NaCl and NaI; see, e.g., $\Sigma = -60$ mC/m^2 in Fig. 2(b). All these observations are in contrast with Derjaguin's treatment of thermoelectricity in charged liquids, which predicts $M_{\mathrm{TE}} \propto \Sigma^3$ [37,38].

We will now try to capture these numerical results theoretically. Our starting point is the expression of the

excess enthalpy density $\delta h(z)$ in Eq. (2), which for electrolytes can be decomposed in two terms:

$$\delta h(z) = \delta h_{\mathrm{wat}}(z) + \delta h_{\mathrm{EDL}}(z). \quad (3)$$

The first term corresponds to the excess enthalpy of water molecules, and is commonly neglected in treatments of thermoelectricity [37,38], and the second term is related to the EDL. This latter contribution can be decomposed into three terms:

$$\delta h_{\mathrm{EDL}}(z) = \delta h_{\mathrm{el}}(z) + \delta h_{\mathrm{osm}}(z) + \delta h_{\mathrm{solv}}(z). \quad (4)$$

The first term, δh_{el}, has an electrostatic origin, and is the one considered in the standard picture; the second term, δh_{osm}, originates from the osmotic pressure of the counterions; and the last term, δh_{solv}, arises from the solvation enthalpy of the ions. The expression of the electrostatic and osmotic excess enthalpy is given in Ref. [44], and in the following we concentrate on the solvation term, as it will be shown to be larger than the two other EDL contributions. In the limit of separate EDLs, the solvation excess enthalpy writes:

$$\delta h_{\mathrm{solv}}(z) = h^+\{n^+(z) - n_b^+\} + h^-\{n^-(z) - n_b^-\}, \quad (5)$$

where $n^{\pm}(z)$ denote the ion number density, $n_b^{\pm}$ their bulk value, and $h^{\pm}$ the ion solvation enthalpy. Here we used the bulk values of $h^{\pm}$ to estimate the solvation term of all the ions. Figure 2(a) shows the three EDL contributions to the thermoelectric coefficient for NaCl solutions. The electrostatic part and the osmotic part are smaller than the simulation results, by 2 and 1 order of magnitude, respectively. This implies that the thermoelectric response of the confined electrolyte is much larger than what is predicted by the standard picture. The solvation term is much larger than the other EDL contributions, but still smaller in amplitude than the computed M_{TE}. Let us now estimate the water contribution in Eq. (3). To that aim, we used the enthalpy profile as computed in additional simulations on a system of pure confined water, keeping all the other parameters constant. In order to calculate the resulting coefficient M_{TE}, we convoluted this approximate excess enthalpy with the EO velocity obtained from the simulations. Figure 2(a) shows that the water contribution is dominant over the EDL terms, and is of the same order of magnitude as the NaCl simulation results. The water term provides a good description of the simulated M_{TE} for negatively charged surfaces. However, it tends to overestimate $|M_{\mathrm{TE}}|$ for positively charged surfaces and also for negative highly charged surfaces. Hence, the water term does not capture all the complexity of the thermoelectric response of the confined liquid.

To confirm this statement, we have added to δh_w the solvation term δh_{solv} and compared to the simulation results for both NaCl and NaI in Fig. 2(b). The corresponding solvation term is calculated beyond the Poisson-Boltzmann approximation, by directly using the simulated ionic density profile. For NaCl, the agreement is very good over the range of Σ considered, while for NaI the agreement is only partial. This partial agreement may be explained by the fact that both the water and solvation terms are approximate, in so far as we used bulk enthalpies to describe the solvation of confined ions, and the water term is calculated for a pure water system. Nevertheless, from Figs. 2(a) and 2(b) we conclude that the thermoelectric response of the confined electrolyte is dominated by the water contribution, and to a lesser extent by the solvation contribution.

Apart from the excess enthalpy density, the thermoelectric response is intimately related to the EO mobility, usually quantified in terms of the so-called ζ potential through the Helmholtz-Smoluchowski (HS) equation [14,75]: $v_{\mathrm{EO}} = -(\varepsilon/\eta)\zeta E_x$, with ε and η the bulk permittivity and shear viscosity, respectively. The EO mobility can be amplified by the liquid-solid slip [7,14,73,76], which is quantified by the slip length b (the extrapolated depth where the no-slip boundary condition would apply). This amplification has been studied theoretically [76–79] and experimentally [80,81], showing that the ζ potential writes $\zeta = \phi_0 + \Sigma b/\varepsilon$, with ϕ_0 the surface potential. We estimated ζ following the experimental procedure, by computing the EO velocity under an electric field and applying the HS equation [44]. Figure 2(c) shows its nonmonotonic behavior as a function of the surface charge, which is due to the decrease of the slip length b with Σ [43,79,82,83]. This complex behavior of ζ in combination with the excess enthalpy density profile results in the nonmonotonic and asymmetrical behavior of M_{TE}.

Through the EO mobility, the thermoelectric response can also be enhanced by slip. To illustrate this point, we focused on NaCl and a homogeneous charge of $-30\ \mathrm{mC/m^2}$, and we tuned the liquid-solid slip by considering surfaces with different wetting properties: one hydrophilic ($\theta \sim 60°$) with a low slip length of ca. 0.2 nm, and another very hydrophobic ($\theta \sim 180°$) with a large slip length of ca. 6.8 nm (details on contact angle estimation can be found in Ref. [44]). Although the original hydrophobic and the very hydrophobic surfaces might appear unrealistic in terms of wetting, the values of slip lengths we obtained are measured experimentally on moderately hydrophobic surfaces [7], and even larger slip lengths have been observed on new 2D materials or in nanotubes [84–87]. Moreover, the amplitude of the interfacial enthalpy excess did not change much when we increased the contact angle from ~60° to almost 180°, so that the thermoelectric responses computed in this work—controlled by both the interfacial enthalpy excess and liquid-solid slip—should not be unrealistic. For the low-slip surface we obtained a very small value of $M_{\mathrm{TE}} = -0.32 \pm 0.05\ \mathrm{C/(ms)}$.

In contrast, we obtained a very large value of $M_{\mathrm{TE}} = 21.45 \pm 0.54$ C/(m s) on the high-slip surface. Liquid-solid slip therefore represents a powerful lever to optimize thermoelectric conversion in nanofluidic systems.

All the results discussed so far concern systems characterized by a uniform surface charge distribution, mimicking, e.g., a polarized surface. However, surface charge can also result from randomly distributed charged groups, e.g., on silica. Therefore, we also simulated heterogeneously charged surfaces, and for both NaCl and NaI solutions, the values of M_{TE} were smaller by typically a factor of 10 [44]. Note that the excess enthalpy density profiles remained similar between homogeneous and heterogeneous surfaces, and that the decrease of M_{TE} can be mostly related to different hydrodynamic boundary conditions [44].

Finally, we focus on the energy harvesting applications of such nanofluidic systems. We evaluate the performance of thermoelectric energy conversion with nanofluidic devices, by computing their Seebeck coefficient S_e, and their so-called figure of merit denoted ZT, traditionally used to quantify the performance of thermoelectric materials. The Seebeck coefficient is defined as $S_e = -\nabla V/\nabla T$ when $j_e = 0$. It then results from Eq. (1) that $S_e = M_{\mathrm{TE}}/(\sigma T)$. ZT is expressed as a function of the Seebeck coefficient S_e, the thermal conductivity, the electric conductivity, and the temperature: $ZT = \sigma S_e^2 T/\kappa$. The figure of merit can equivalently be expressed as a function of the thermoelectric coefficient M_{TE}: $ZT = M_{\mathrm{TE}}^2/(\sigma\kappa T)$. To quantify the expected experimental figure of merit, we assume in the following that the solid walls may be chosen in order to have limited influence on the device thermoelectric response. In particular, we use the experimental thermal conductivity of water, $\kappa_{\mathrm{wat}} = 0.609$ W m^{-1} K^{-1}, and we assume that the solid walls are electric insulators with a negligible thermoelectric response, so that the electric conductivity σ and thermoelectric coefficient M_{TE} are those of the confined liquid, computed in the simulations.

Figure 3 displays the computed ZT and S_e against the surface charge density, for the same systems studied in Fig. 2. NaCl generally offers better performance than NaI. A maximum ZT of ca. 0.1 is obtained for $\Sigma = -15$ mC/m^2, corresponding to a Seebeck coefficient of ca. 10 mV/K. In a recent theoretical work [30], $|S_e|$ originating from the electrostatic term was estimated to be ca. 0.2 mV/K in a confined fluidic system, with a similar ζ potential and the same ratio of the slit gap to the Debye length. Other simulation studies evaluated the Seebeck coefficient of bulk electrolyte solutions [32,33], and found absolute values of up to ~0.1 mV/K. Our maximum value also exceeds the experimental data on ion-exchange membrane systems reviewed in Ref. [26] by one order of magnitude. Note that the large thermoelectric effects observed here are specific to the nanoscale. Indeed, as

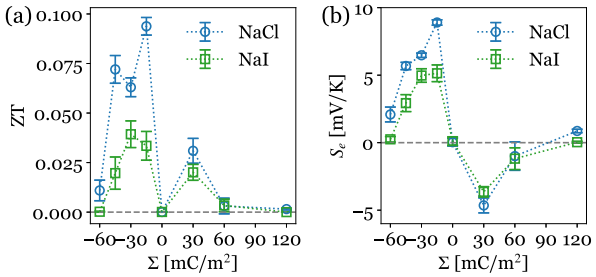

FIG. 3. (a) Figure of merit ZT and (b) corresponding Seebeck coefficient S_e against the surface charge density Σ, for the same systems studied in Fig. 2.

detailed in Ref. [44], M_{TE} and ZT should decrease with the channel size d, and vanish in macroscopic pores.

However, there is still room to enhance the thermoelectric performance of nanofluidic devices, by addressing several key factors appearing in ZT. First, we have shown that a large slip length b results in high EO mobility and thermoelectric coefficient, so high-slip surfaces are preferred. Second, in contrast with the traditional solid thermoelectric materials, a small electrical conductivity is favorable to enhance ZT, for a given M_{TE}. Since thermoelectric transport arises from the counterions at the interface, the only way to reduce the electric conductivity is by reducing the ion concentration in the bulk. To assess that point, we conducted an additional set of simulations on a salt-free system containing only counterions, with the most hydrophobic and homogeneously charged surface tested above. For $\Sigma = -30$ mC/m^2, we obtained a high ZT of ca. 2.7, comparable to that of the best performing room temperature thermoelectric materials such as nanostructured Bi_2Te_3 and Bi_2Se_3. Of course this giant ZT was obtained for a somewhat ideal system, with homogeneous surface charge and large slip length. However, in real systems where it might be difficult to combine a large, heterogeneous surface charge with a large slip length, we suggest that many other potential levers remain to be explored in order to optimize the heat harvesting performance. As a simple example, we have shown that the interfacial enthalpy excess of the solvent plays a key role. One could then add a (neutral) solute to affect the bulk (and interfacial) enthalpy density of water in order to enhance the interfacial enthalpy excess.

Summary.—We computed the thermoelectric coefficient using MD simulations for a model nanofluidic system with electrolyte solutions and charged solid walls. We showed that the standard electrostatic picture of the EDL cannot describe the global thermoelectric transport in nanofluidic systems. First, compared to the ion solvation enthalpy, the electrostatic and osmotic contributions induced by the EDL were found to be negligible. Second, we outlined the dominant role of water molecules enthalpy in the thermoelectric transport of the electrolyte, which is neglected in the standard picture. Finally, hydrodynamic slip can largely

enhance the thermoelectric coefficient, and should be taken into account in the modeling and engineering of such transport process. In particular, we showed that the spatial distribution of the surface charge has a strong impact on slip, and hence on the thermoelectric coefficient. Better performance was obtained for a homogeneous surface charge, representative of, e.g., polarized surfaces. We also investigated the heat harvesting efficiency displayed by these nanofluidic systems by computing the so-called figure of merit and the Seebeck coefficient. We discussed the interest of reducing the salt concentration, and we showed that figures of merit comparable to those of state-of-the-art solid-state thermoelectric materials could be obtained in the salt-free limit. Although our simple model neglects practical effects that could limit the performance of experimental systems, we hope our results will motivate further theoretical and experimental work toward the realization of efficient nanofluidic waste heat harvesters.

The authors thank A.-L. Biance, C. Ybert, and C. Cottin-Bizonne for fruitful discussions. This work is supported by the ANR, Project No. ANR-16-CE06-0004-01 NECtAR. L. J. is supported by the Institut Universitaire de France. S. M. acknowledges support from the H2020 programme FET-open project EFINED (Project No. 766853).

*laurent.joly@univ-lyon1.fr
†samy.merabia@univ-lyon1.fr

[1] W. Sparreboom, A. van den Berg, and J. C. T. Eijkel, Nat. Nanotechnol. **4**, 713 (2009).
[2] L. Bocquet and P. Tabeling, Lab Chip **14**, 3143 (2014).
[3] A. Siria, P. Poncharal, A.-L. Biance, R. Fulcrand, X. Blase, S. T. Purcell, and L. Bocquet, Nature (London) **494**, 455 (2013).
[4] J. Feng, M. Graf, K. Liu, D. Ovchinnikov, D. Dumcenco, M. Heiranian, V. Nandigana, N. R. Aluru, A. Kis, and A. Radenovic, Nature (London) **536**, 197 (2016).
[5] A. Siria, M.-L. Bocquet, and L. Bocquet, Nat. Rev. Chem. **1**, 0091 (2017).
[6] J. Anderson, Annu. Rev. Fluid Mech. **21**, 61 (1989).
[7] L. Bocquet and E. Charlaix, Chem. Soc. Rev. **39**, 1073 (2010).
[8] D. Andelman, *Handbook of Biological Physics* Vol. 1 (Elsevier, North-Holland, 1995), pp. 603–642.
[9] J. N. Israelachvili, *Intermolecular and Surface Forces* (Academic Press, Amsterdam, 2011), p. 674.
[10] *Solid-Liquid Interfaces*, edited by J. Lyklema, Fundamentals of Interface and Colloid Science Vol. 2 (Academic Press, 1995), p. iii.
[11] F. H. J. van der Heyden, D. J. Bonthuis, D. Stein, C. Meyer, and C. Dekker, Nano Lett. **6**, 2232 (2006).
[12] S. Pennathur, J. C. T. Eijkel, and A. van den Berg, Lab Chip **7**, 1234 (2007).
[13] I. Pagonabarraga, B. Rotenberg, and D. Frenkel, Phys. Chem. Chem. Phys. **12**, 9566 (2010).
[14] R. Hartkamp, A.-L. Biance, L. Fu, J.-F. Dufrêche, O. Bonhomme, and L. Joly, Curr. Opin. Colloid Interface Sci. **37**, 101 (2018).
[15] G. Xue, Y. Xu, T. Ding, J. Li, J. Yin, W. Fei, Y. Cao, J. Yu, L. Yuan, L. Gong *et al.*, Nat. Nanotechnol. **12**, 317 (2017).
[16] O. Bonhomme, B. Blanc, L. Joly, C. Ybert, and A.-L. Biance, Adv. Colloid Interface Sci. **247**, 477 (2017).
[17] B. Blanc, O. Bonhomme, P.-F. Brevet, E. Benichou, C. Ybert, and A.-L. Biance, Soft Matter **14**, 2604 (2018).
[18] C. Zhao and C. Yang, Adv. Colloid Interface Sci. **201–202**, 94 (2013).
[19] Y. Xie, J. D. Sherwood, L. Shui, A. van den Berg, and J. C. Eijkel, Lab Chip **11**, 4006 (2011).
[20] F. Liu, A. Klaassen, C. Zhao, F. Mugele, and D. van den Ende, J. Phys. Chem. B **122**, 933 (2018).
[21] A. Ajdari and L. Bocquet, Phys. Rev. Lett. **96**, 186102 (2006).
[22] Y. Ren and D. Stein, Nanotechnology **19**, 195707 (2008).
[23] D. J. Rankin and D. M. Huang, Langmuir **32**, 3420 (2016).
[24] M. Bonetti, S. Nakamae, B. T. Huang, T. J. Salez, C. Wiertel-Gasquet, and M. Roger, J. Chem. Phys. **142**, 244708 (2015).
[25] B. T. Huang, M. Roger, M. Bonetti, T. J. Salez, C. Wiertel-Gasquet, E. Dubois, R. Cabreira Gomes, G. Demouchy, G. Mériguet, V. Peyre, M. Kouyaté, C. L. Filomeno, J. Depeyrot, F. A. Tourinho, R. Perzynski, and S. Nakamae, J. Chem. Phys. **143**, 054902 (2015).
[26] V. Barragán, K. Kristiansen, and S. Kjelstrup, Entropy **20**, 905 (2018).
[27] T. Salez, S. Nakamae, R. Perzynski, G. Mériguet, A. Cebers, and M. Roger, Entropy **20**, 405 (2018).
[28] K. R. Kristiansen, V. M. Barragán, and S. Kjelstrup, Phys. Rev. Applied **11**, 044037 (2019).
[29] T. Li, X. Zhang, S. D. Lacey, R. Mi, X. Zhao, F. Jiang, J. Song, Z. Liu, G. Chen, J. Dai, Y. Yao, S. Das, R. Yang, R. M. Briber, and L. Hu, Nat. Mater. **18**, 608 (2019).
[30] M. Dietzel and S. Hardt, Phys. Rev. Lett. **116**, 225901 (2016).
[31] M. Dietzel and S. Hardt, J. Fluid Mech. **813**, 1060 (2017).
[32] S. Di Lecce, T. Albrecht, and F. Bresme, Sci. Rep. **7**, 44833 (2017).
[33] S. Di Lecce and F. Bresme, J. Phys. Chem. B **122**, 1662 (2018).
[34] A. Ly, A. Majee, and A. Würger, New J. Phys. **20**, 025001 (2018).
[35] L. Li and Q. Wang, Small **14**, 1800369 (2018).
[36] W. Zhang, Q. Wang, and C. Zhao, arXiv:1805.03462.
[37] B. V. Derjaguin, Pure Appl. Chem. **52**, 1163 (1980).
[38] B. V. Derjaguin, N. V. Churaev, and V. M. Muller, Surface forces in transport phenomena, in *Surface Forces* (Springer US, Boston, MA, 1987), pp. 369–431.
[39] S. R. De Groot and P. Mazur, *Non-Equilibrium Thermodynamics* (Dover Publications, New York, 1984).
[40] E. Brunet and A. Ajdari, Phys. Rev. E **69**, 016306 (2004).
[41] S. Plimpton, J. Comput. Phys. **117**, 1 (1995).
[42] D. M. Huang, C. Cottin-Bizonne, C. Ybert, and L. Bocquet, Phys. Rev. Lett. **98**, 177801 (2007).
[43] D. M. Huang, C. Cottin-Bizonne, C. Ybert, and L. Bocquet, Langmuir **24**, 1442 (2008).
[44] See Supplemental Material at http://link.aps.org/supplemental/10.1103/PhysRevLett.123.138001 for further details, which includes Refs. [45–63].

[45] A. I. Jewett, Z. Zhuang, and J.-E. Shea, Biophys. J. **104**, 169a (2013).
[46] W. Humphrey, A. Dalke, and K. Schulten, J. Mol. Graphics **14**, 33 (1996).
[47] A. Kohlmeyer, Topotools, https://zenodo.org/badge/latestdoi/13922095.
[48] I. V. Leontyev and A. A. Stuchebrukhov, J. Chem. Phys. **130**, 085102 (2009).
[49] I. Leontyev and A. Stuchebrukhov, Phys. Chem. Chem. Phys. **13**, 2613 (2011).
[50] M. Kohagen, P. E. Mason, and P. Jungwirth, J. Phys. Chem. B **118**, 7902 (2014).
[51] M. Kohagen, P. E. Mason, and P. Jungwirth, J. Phys. Chem. B **120**, 1454 (2016).
[52] A. L. Benavides, M. A. Portillo, V. C. Chamorro, J. R. Espinosa, J. L. F. Abascal, and C. Vega, J. Chem. Phys. **147**, 104501 (2017).
[53] T. Martinek, E. Duboué-Dijon, Š. Timr, P. E. Mason, K. Baxová, H. E. Fischer, B. Schmidt, E. Pluhaová, and P. Jungwirth, J. Chem. Phys. **148**, 222813 (2018).
[54] W. R. Smith, I. Nezbeda, J. Kolafa, and F. Moučka, Fluid Phase Equilib. **466**, 19 (2018).
[55] R. Renou, M. Ding, H. Zhu, A. Szymczyk, P. Malfreyt, and A. Ghoufi, J. Phys. Chem. B **118**, 3931 (2014).
[56] E. E. Bruce and N. F. A. van der Vegt, J. Chem. Phys. **148**, 222816 (2018).
[57] D. Biriukov, O. Kroutil, and M. Pedota, Phys. Chem. Chem. Phys. **20**, 23954 (2018).
[58] I.-C. Yeh and M. L. Berkowitz, J. Chem. Phys. **111**, 3155 (1999).
[59] J.-L. Barrat and L. Bocquet, Phys. Rev. Lett. **82**, 4671 (1999).
[60] T. Werder, J. H. Walther, R. L. Jaffe, T. Halicioglu, and P. Koumoutsakos, J. Phys. Chem. B **107**, 1345 (2003).
[61] A. Würger, Rep. Prog. Phys. **73**, 126601 (2010).
[62] M. Janssen and R. van Roij, Phys. Rev. Lett. **118**, 096001 (2017).
[63] A. Rashin and B. Honig, J. Phys. Chem. **89**, 5588 (1985).
[64] J. L. F. Abascal and C. Vega, J. Chem. Phys. **123**, 234505 (2005).
[65] Z. R. Kann and J. L. Skinner, J. Chem. Phys. **141**, 104507 (2014).
[66] L. Fu, S. Merabia, and L. Joly, Phys. Rev. Lett. **119**, 606 (2017).
[67] L. Fu, S. Merabia, and L. Joly, J. Phys. Chem. Lett. **9**, 2086 (2018).
[68] L. Joly, F. Detcheverry, and A.-L. Biance, Phys. Rev. Lett. **113**, 088301 (2014).
[69] H. Yoshida, H. Mizuno, T. Kinjo, H. Washizu, and J.-L. Barrat, J. Chem. Phys. **140**, 214701 (2014).
[70] M. Předota, M. L. Machesky, and D. J. Wesolowski, Langmuir **32**, 10189 (2016).
[71] J. B. Freund, J. Chem. Phys. **116**, 2194 (2002).
[72] R. Qiao and N. R. Aluru, Phys. Rev. Lett. **92**, 198301 (2004).
[73] V. Marry, J.-F. Dufrêche, M. Jardat, and P. Turq, Mol. Phys. **101**, 3111 (2003).
[74] J.-F. Dufrêche, V. Marry, N. Malikova, and P. Turq, J. Mol. Liq. **118**, 145 (2005).
[75] A. V. Delgado, F. González-Caballero, R. J. Hunter, L. K. Koopal, and J. Lyklema, J. Colloid Interface Sci. **309**, 194 (2007).
[76] L. Joly, C. Ybert, E. Trizac, and L. Bocquet, Phys. Rev. Lett. **93**, 257805 (2004).
[77] V. M. Muller, I. P. Sergeeva, V. D. Sobolev, and N. V. Churaev, Colloid J. USSR **48**, 606 (1986).
[78] H. A. Stone, A. D. Stroock, and A. Ajdari, Annu. Rev. Fluid Mech. **36**, 381 (2004).
[79] L. Joly, C. Ybert, E. Trizac, and L. Bocquet, J. Chem. Phys. **125**, 204716 (2006).
[80] C. I. Bouzigues, P. Tabeling, and L. Bocquet, Phys. Rev. Lett. **101**, 114503 (2008).
[81] M.-C. Audry, A. Piednoir, P. Joseph, and E. Charlaix, Faraday Discuss. **146**, 113 (2010).
[82] A. Botan, V. Marry, B. Rotenberg, P. Turq, and B. Noetinger, J. Phys. Chem. C **117**, 978 (2013).
[83] D. Jing and B. Bhushan, J. Colloid Interface Sci. **454**, 152 (2015).
[84] M. Majumder, N. Chopra, R. Andrews, and B. J. Hinds, Nature (London) **438**, 44 (2005).
[85] J. K. Holt, Science **312**, 1034 (2006).
[86] A. Maali, T. Cohen-Bouhacina, and H. Kellay, Appl. Phys. Lett. **92**, 053101 (2008).
[87] E. Secchi, S. Marbach, A. Niguès, D. Stein, A. Siria, and L. Bocquet, Nature (London) **537**, 210 (2016).